Research Article Vol. 30, No. 4 / 14 Feb 2022 / Optics Express 5553
Optics EXPRESS

Continuous multi-step pumping of the optical clock transition in alkaline-earth atoms with minimal perturbation

CHRISTOPH HOTTER,[1,*] DAVID PLANKENSTEINER,[1] GEORGY KAZAKOV,[2] AND HELMUT RITSCH[1]

[1] *Institut für Theoretische Physik, Universität Innsbruck, Technikerstr. 21a, A-6020 Innsbruck, Austria*
[2] *Atominstitut, TU Wien, Stadionallee 2, 1020 Vienna, Austria*
[*] *christoph.hotter@uibk.ac.at*

Abstract: A suitable scheme to continuously create inversion on an optical clock transition with negligible perturbation is a key missing ingredient required to build an active optical atomic clock. Repumping of the atoms on the narrow transition typically needs several pump lasers in a multi step process involving several auxiliary levels. In general this creates large effective level shifts and a line broadening, strongly limiting clock accuracy. Here we present an extensive theoretical study for a realistic multi-level implementation in search of parameter regimes where a sufficient inversion can be achieved with minimal perturbations. Fortunately we are able to identify a useful operating regime, where the frequency shifts remain small and controllable, only weakly perturbing the clock transition for useful pumping rates. For practical estimates of the corresponding clock performance, we introduce a straightforward mapping of the multilevel pump scheme to an effective energy shift and broadening of parameters for the reduced two-level laser model system. This allows us to evaluate the resulting laser power and spectrum using well-known methods.

1. Introduction

State of the art optical atomic lattice clocks achieve an excellent fractional stability of up to 6.6×10^{-19} after one hour of averaging [1]. In a typical atomic clock a stable local laser oscillator is compared to the reference transition frequency of trapped ultra-cold atoms. Technically the local laser oscillator is stabilized by an ultra-stable macroscopic cavity with a very good short time stability. Limitations of its stability originate from length fluctuations due to environmental and thermal perturbations [2]. Currently, these perturbations are the central limiting factor of the performance of passive atomic clocks on the short timescale. It has been proposed [3,4] that active optical clocks, realized as so called superradiant lasers [3–31], can overcome this limitation. In such a laser an ensemble of atoms with a narrow and stable transition is used as gain medium inside an optical resonator. Since the cavity bandwidth is much broader than the gain profile, the frequency of such a bad-cavity laser is primarily determined by the stability of the resonance frequency of the gain medium which makes the system robust against cavity length fluctuations.

Maintaining population inversion on the atomic clock transition is, of course, a necessary ingredient required for continuous operation of an active optical clock laser. One possibility to achieve this is to prepare the atoms in the upper lasing state outside of the active lasing region and subsequently injecting them into the cavity. Such an approach is reminiscent of the hydrogen maser [32,33]. In the optical regime this can be realized, for example, as an atomic beam laser [3,18,34,35], where atoms in the upper lasing state traverse the cavity. However, a continuous replenishment of cold atoms prepared in the upper lasing state with a large enough rate is a challenging task [35]. By repumping the laser active atoms trapped within a magic wavelength

#445976 https://doi.org/10.1364/OE.445976
Journal © 2022 Received 18 Oct 2021; revised 17 Dec 2021; accepted 3 Jan 2022; published 7 Feb 2022

Optics EXPRESS

optical lattice inside the cavity [4–6,19,21,36,37], however, each atom can emit several photons into the cavity. Thus for a continuous operation the atomic flux only needs to compensate the lost atoms and hence can be significantly reduced. This could be e.g. achieved with an optical conveyor lattice through the cavity [13,14,35,38,39]. The central challenge of this approach are the perturbations of the clock atoms due to the presence of the repumping lasers. Typical theoretical models dedicated to superradiant clock lasers with continuous repumping simply assume an artificial transition rate modelled as inverse spontaneous decay from the ground to the excited lasing state [4,11,19–21]. This introduces an effective homogeneous broadening of the laser line but ignores all shifts and inhomogeneous broadening. To model this in a more realistic scheme, however, one needs to introduce laser-induced transitions to some auxiliary intermediate levels followed by a spontaneous decay to the upper lasing state. Naturally these lasers will introduce differential light shifts in addition to decoherence on the clock transition. For a non-uniform pump laser field distribution one, of course, gets inhomogeneous broadening. Besides broadening and shifting the laser line, it will eventually modify the threshold and even inhibit lasing. Frequency shifts lead to additional inaccuracy at least if they are not controllable and precisely measurable, as the resulting laser frequency then differs from the bare atomic transition. Luckily, as long as the inhomogeneous broadening is sufficiently small and symmetric, the atoms with different energies still synchronize [7,15,30] and a narrow laser linewidth can be maintained. Therefore, the design of high-performance active optical clocks with a continuous repumping scheme requires the characterization, control and, if possible, minimization of the induced shifts and resulting decoherence.

The conceptually simplest realistic repumping scheme, the so-called three-level scheme, includes only a single intermediate level coherently coupled to the laser ground state, which ideally directly decays to the upper lasing level on a short time scale. Its theoretical study can be drastically simplified when the auxiliary level can be adiabatically eliminated, reducing the model to an effective two-level system subject to an effective incoherent pump, as e.g. in Lu^+ ions [16]. The Stark shift of the lasing transition can be effectively added to the model. However, in most metrology-relevant neutral atoms, as e.g. strontium or ytterbium, such an ideal intermediate level does not exist and thus any realistic repumping scheme requires at least two laser-induced transition steps to irreversibly excite the atoms from the lower to the upper clock state. This has the advantage that one has more possibilities to obtain a desired pump rate with minimal perturbation. However, it has also the disadvantage that, on the one hand, an analytic procedure of adiabatic elimination is cumbersome, especially for systems with a complex multilevel structure. On the other hand, a full numerical treatment, including all the relevant levels in the laser model, significantly increases the computational cost. Especially in time-domain simulations the characteristic time constants of the laser active and intermediate states often differ by many orders of magnitude, requiring a large number of time steps to be calculated.

Of course the numerical challenges become even more prominent for calculations beyond the mean-field approximation as needed for reliable predictions of linewidth and stability. As particularly useful models to tackle this, we will employ higher order cumulant expansion methods [40,41]. Luckily we see that, as in the three level case, adiabatic elimination of the intermediate levels can reduce these multi-level systems to a simplified effective two-level system with sufficient accuracy.

In this paper we consider a quite general multi-level repumping scheme for neutral ^{88}Sr. We demonstrate that a proper choice of intensities and detunings of the pump lasers can lead to a sufficiently high effective repumping rate while at the same time frequency shifts and decoherence rates are kept small. To perform this analysis, we introduce a numerical method to reduce the complex multi-level system to an effective two-level system. This work is organized as follows: In Section 2 we review the simplified two-level model including incoherent repumping, and

Optics EXPRESS

describe the generalized method used to reduce a multilevel system to a two-level one. In Section 3 we introduce a repumping scheme for trapped ^{88}Sr and calculate the effective parameters of the equivalent two-level system. The pumping scheme includes the two lasing states and four intermediate states. In Section 4 we compare the effective two-level laser model with the full six-level laser model.

2. Multistep excitation process as an effective two-level system

In this section we describe the method to eliminate the intermediate states in a multilevel scheme with continuous repumping to an effective two-level system by using the eigenvalues of the non-hermitian Hamiltonian. The requirement on this procedure is that the intermediates states can be adiabatically eliminated. The motivation for this procedure is that the full laser system can be numerically very extensive for multilevel systems, and a "conventional" adiabatic elimination is often too cumbersome to be handled analytically. With our method we numerically calculate first the appropriate parameters of an equivalent two-level atom, to use them afterwards in an effective laser model. This has the additional advantage that this simplified model has already been studied extensively [4,6,7,20,21].

To establish the correspondence between the effective two-level and the multilevel system, we investigate first a two-level atom subjected to spontaneous decay, decoherence and incoherent pumping. In the Heisenberg representation the averaged value of an operator $\hat{O}$ for an open quantum system follows the equation

$$\frac{d\langle\hat{O}\rangle}{dt} = \frac{i}{\hbar}\langle[\hat{H},\hat{O}]\rangle + \langle\hat{\hat{\mathcal{L}}}[\hat{O}]\rangle \tag{1}$$

where $\hat{H}$ is the Hamiltonian and $\hat{\hat{\mathcal{L}}}$ is the super-operator describing the dissipative processes. Within the Born-Markov approximation $\hat{\hat{\mathcal{L}}}$ has the form

$$\hat{\hat{\mathcal{L}}}[\hat{O}] = \sum_j \frac{R_j}{2}\left(2\hat{J}_j^\dagger\hat{O}\hat{J}_j - \hat{J}_j^\dagger\hat{J}_j\hat{O} - \hat{O}\hat{J}_j^\dagger\hat{J}_j\right), \tag{2}$$

here $\hat{J}_j$ are the jump operators with the corresponding rates R_j. For our two-level atom in the rotating frame of the unperturbed atomic transition frequency the Hamiltonian can be written as $\hat{H} = \hbar(\delta_1\hat{\sigma}_{11} + \delta_2\hat{\sigma}_{22})$, where δ_1 and δ_2 are the shifts from the ground $|1\rangle$ and excited clock state $|2\rangle$, respectively and $\hat{\sigma}_{ij} = |i\rangle\langle j|$. The jump operators and corresponding rates of the dissipative processes are listed in Table 1. The equations of motion for the operator averages $\langle\hat{\sigma}_{ij}\rangle$ of such a two-level atom are

$$\partial_t\langle\hat{\sigma}_{22}\rangle = R\langle\hat{\sigma}_{11}\rangle - \Gamma_{12}\langle\hat{\sigma}_{22}\rangle \tag{3}$$

$$\partial_t\langle\hat{\sigma}_{12}\rangle = -\left(\frac{R+\Gamma_{12}+\nu}{2} + i\delta_{21}\right)\langle\hat{\sigma}_{12}\rangle, \tag{4}$$

where $\delta_{21} = \delta_2 - \delta_1$, and $\nu = \nu_1 + \nu_2$. From (3) one can easily express the incoherent repumping rate R via the ratio of the steady-state population as

$$R = \frac{\langle\hat{\sigma}_{22}\rangle}{\langle\hat{\sigma}_{11}\rangle}\Gamma_{12}. \tag{5}$$

To express the dephasing rates ν_1 and ν_2 we exploit the effective non-hermitian Hamiltonian

$$\hat{H}_{\text{eff}}^{\text{nh}} = \hat{H} - \frac{i\hbar}{2}\sum_j R_j\hat{J}_j^\dagger\hat{J}_j, \tag{6}$$

Optics EXPRESS

as it is used e.g. in the Monte-Carlo wave function approach [42–44]. For our two-level system this non-hermitian Hamiltonian has the form

$$\hat{H}_{\text{eff}}^{\text{nh}} = \hbar\delta_1\hat{\sigma}_{11} + \hbar\delta_2\hat{\sigma}_{22} - \frac{i\hbar}{2}\left[\Gamma_{12}\hat{\sigma}_{22} + R\hat{\sigma}_{11} + \nu_1\hat{\sigma}_{11} + \nu_2\hat{\sigma}_{22})\right], \tag{7}$$

which is already diagonal with the complex eigenvalues

$$E_1 = \hbar\left[\delta_1 - \frac{i}{2}(R + \nu_1)\right] \tag{8}$$

$$E_2 = \hbar\left[\delta_2 - \frac{i}{2}(\Gamma_{12} + \nu_2)\right]. \tag{9}$$

Using these relations and Eq. (5) for the incoherent pump rate R, we can express the shifts and decoherence rates via the eigenvalues of this effective Hamiltonian as:

$$\begin{aligned}\delta_1 &= \text{Re}\{E_1\}/\hbar\\ \delta_2 &= \text{Re}\{E_2\}/\hbar\\ \nu_1 &= -2\text{Im}\{E_1\}/\hbar - R\\ \nu_2 &= -2\text{Im}\{E_2\}/\hbar - \Gamma_{12}\end{aligned} \tag{10}$$

Table 1. Dissipative processes of the two-level scheme.

#	jump	rate	description
1	$\hat{\sigma}_{12}$	Γ_{12}	decay from $\|2\rangle$ to $\|1\rangle$
2	$\hat{\sigma}_{21}$	R	incoherent pumping from $\|1\rangle$ to $\|2\rangle$
3	$\hat{\sigma}_{11}$	ν_1	dephasing on $\|1\rangle$
4	$\hat{\sigma}_{22}$	ν_2	dephasing on $\|2\rangle$

Therefore, to reduce a driven multilevel system to an effective two-level system with incoherent pumping, we perform the following steps: First, we calculate the steady-state values for $\langle\hat{\sigma}_{11}\rangle$ and $\langle\hat{\sigma}_{22}\rangle$, to obtain the effective repumping rate R from Eq. (5). For the validity of the adiabatic elimination one should check that the condition $1 - \langle\hat{\sigma}_{11}\rangle - \langle\hat{\sigma}_{22}\rangle \ll 1$ is fulfilled at this stage. Second, we diagonalize the effective non-hermitian Hamiltonian (6) to get the complex eigenvalues E_1 and E_2. These eigenvalues correspond to the eigenstates with the highest overlap with the unperturbed clock states $|1\rangle$ and $|2\rangle$. Using these eigenvalues we calculate the shifts δ_1 and δ_2 and the decoherence rates ν_1 and ν_2 according to Eq. (10). In appendix A we apply this method analytically to a three-level system, and compare it to the "conventional" adiabatic elimination procedure. Note that the atoms are coupled to the cavity only on the weak $|1\rangle \leftrightarrow |2\rangle$ transition, which will not be adiabatically eliminated. Therefore the atom-cavity coupling of the reduced system is anyway retained and we can, in a good approximation, neglect the cavity field and perform the adiabatic elimination on a single atom. However, this means that all higher order correlations which include atomic transitions with intermediate levels are neglected. If these correlations become relevant, the approximation might no longer be valid. Also direct interaction between the atoms as well as any collective coupling of the atoms to the bath modes are neglected.

3. Repumping scheme for bosonic strontium

In the following we present the concrete proposed repumping scheme based on the actual level structure of ^{88}Sr, see Fig. 1. In order to allow for superradiant lasing and to keep the anyway

Optics EXPRESS

complicated system as simple as possible, we assume a fairly strong and homogeneous magnetic field $B = 0.18$ T on the atoms, which induces an effective weak electric dipole coupling between the states $|1\rangle = {}^1S_0$ and $|2\rangle = {}^3P_0$ with a spontaneous transition rate of $\Gamma_{12} \approx 2\pi \cdot 1$ mHz. Naturally such a strong magnetic field splits the Zeeman sub-levels quite far, such that they can be addressed independently. To obtain sufficient population in the upper clock state $|2\rangle = {}^3P_0$ we consider the following processes: The atom is pumped coherently from the ground state $|1\rangle = {}^1S_0$ to $|3\rangle = {}^3P_{1,m=-1}$ and then further to $|4\rangle = {}^3S_{1,m=0}$. From there the atom can decay into the upper lasing state $|2\rangle$ as well as into the states $|5\rangle = {}^3P_{2,m=\{-1,0,+1\}}$ and $|6\rangle = {}^3P_{1,m=-1}$. Note that the atoms can not decay from $|4\rangle$ to ${}^3P_{1,m=0}$, since this transition is forbidden by angular momentum selection rules. Furthermore we combine here the three relevant Zeeman sub-levels of the state ${}^3P_2$ to one state $|5\rangle$, this does not change the dynamics of the system, but one needs to be aware that in real experiments three individual lasers are needed to repump the atoms from these levels.

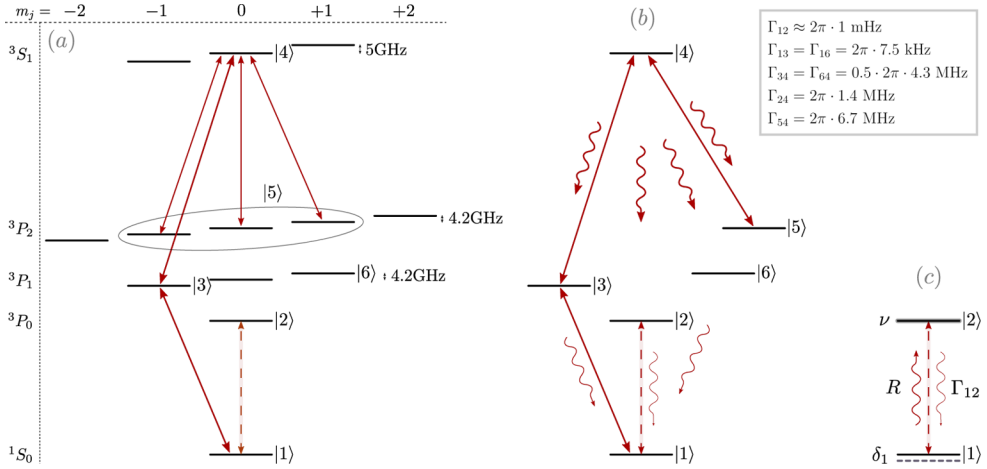

Fig. 1. *Effective pump schemes:* Figure (a) shows all relevant atomic levels involved in CW pumping including the Zeeman sub-levels. Numbers show the level shifts for $B = 0.18$T. The directly involved transitions are indicated by the red solid lines. Figure (b) depicts a simplified six-level pump scheme with the relevant decay rates. (c) describes the resulting reduced two-level laser model including the effective emerging incoherent pump rate R and ground state Stark shift δ_1. We also include an effective dephasing with rate ν on the lasing transition. The cavity coupling is indicated by the dashed line between $|1\rangle$ and $|2\rangle$. The decay rates are from [45].

The decay $|4\rangle \rightarrow |2\rangle$ is the desired final step in the excitation process. Since the state $|5\rangle$ has a lifetime even longer than the upper clock state, we need to additionally depopulate $|5\rangle$ to avoid trapping of too much population in this state. If the atoms decay into the state $|6\rangle$, we can either repump it back to the state $|4\rangle$, or simply let it decay further to the ground state. Pumping from the state $|6\rangle$ would further increase the efficiency of the repumping process, but for simplicity we just consider spontaneous decay to the ground state. The Hamiltonian for the pumped six-level scheme (Fig. 1(b)) in the rotating frame of the pump lasers then is

$$\hat{H}_\mathrm{p} = -\Delta_3\hat{\sigma}_{33} - \Delta_4\hat{\sigma}_{44} - \Delta_5\hat{\sigma}_{55} + \Omega_{13}(\hat{\sigma}_{13} + \hat{\sigma}_{31}) + \Omega_{34}(\hat{\sigma}_{34} + \hat{\sigma}_{43}) + \Omega_{54}(\hat{\sigma}_{45} + \hat{\sigma}_{54}) \quad (11)$$

with $\Delta_3 = \Delta_{13}$, $\Delta_4 = \Delta_3 + \Delta_{34}$ and $\Delta_5 = \Delta_4 - \Delta_{54}$. We define here $\Delta_{ij} = \omega_{ij}^l - \omega_{ij}$, ω_{ij} is the resonance frequency on the atomic transition $|i\rangle \leftrightarrow |j\rangle$, ω_{ij}^l is the frequency of the pump laser on this transition and Ω_{ij} the matrix element of the laser-induced transition. Dissipative

Optics EXPRESS

processes for this pump scheme are described by the Liouvillian (2) with the parameters listed in Table 2. These processes include all the relevant atomic decays, an effective phenomenological dephasing of the clock transition, as well as the dephasing induced by the pump lasers due to a finite linewidth. We want to mention here that the considered 6-level model is only valid due to the strong magnetic field, which resolves the Zeeman sublevels. However, for a weaker magnetic field, or also for fermionic ^{87}Sr the method can still be applied as long as one includes all relevant levels. Furthermore we should also note that in our scheme the atoms emit and absorb approximately 22 photons on average in one repumping cycle. All these photons have a wavelength around 700 nm which leads to heating of about 5 μK per cycle. Assuming an optical lattice potential with a depth of $k_B \cdot 30$ μK, the atoms can emit a few photons into the cavity before heated out of the trap. This could be significantly improved by additional cooling of the atoms, e.g. on the narrow cyclic $^3P_2 \leftrightarrow {}^3D_3$ transition at a wavelength of 2.9 μm.

Table 2. Dissipative processes of the six-level pump scheme.

#	jump	rate	description
1	$\hat{\sigma}_{12}$	Γ_{12}	decay from $\|2\rangle$ to $\|1\rangle$
2	$\hat{\sigma}_{13}$	Γ_{13}	decay from $\|3\rangle$ to $\|1\rangle$
3	$\hat{\sigma}_{34}$	Γ_{34}	decay from $\|4\rangle$ to $\|3\rangle$
4	$\hat{\sigma}_{24}$	Γ_{24}	decay from $\|4\rangle$ to $\|2\rangle$
5	$\hat{\sigma}_{54}$	Γ_{54}	decay from $\|4\rangle$ to $\|5\rangle$
6	$\hat{\sigma}_{64}$	Γ_{64}	decay from $\|4\rangle$ to $\|6\rangle$
7	$\hat{\sigma}_{16}$	Γ_{16}	decay from $\|6\rangle$ to $\|1\rangle$
8	$\hat{\sigma}_{22}$	ν_{12}	general dephasing on $\|1\rangle \leftrightarrow \|2\rangle$
9	$\hat{\sigma}_{33} + \hat{\sigma}_{44} + \hat{\sigma}_{55}$	ν_{13}	pump laser linewidth on $\|1\rangle \leftrightarrow \|3\rangle$
10	$\hat{\sigma}_{44} + \hat{\sigma}_{55}$	ν_{34}	pump laser linewidth on $\|3\rangle \leftrightarrow \|4\rangle$
11	$\hat{\sigma}_{55}$	ν_{54}	pump laser linewidth on $\|4\rangle \leftrightarrow \|5\rangle$

3.1. Scanning over repumping parameters

Using the method described in section 2 we analyze our Strontium six-level repumping scheme. For high atom numbers $N \gg 1$ an effective incoherent repumping rate R above Γ_{12} would already be sufficient for superradiant lasing [4,15]. A larger rate, however, leads to a higher output power and smaller linewidth, with an optimum at $R = 2Ng^2/\kappa$ [4]. Here g is the atom cavity coupling constant and κ the photon decay rate through the cavity mirrors. We will focus on incoherent repumping rates $R > 2\pi \cdot 1$ Hz, which is obviously much bigger than $\Gamma_{12} = 2\pi \cdot 1$ mHz but not the optimum for usual atom numbers and cavity parameters. The issue with too high repumping rates is, that they usually require stronger pump fields which lead to bigger level shifts on the clock transition. Shifts per se would not be a problem if they are constant and known. However, due to uncertainties and fluctuations in the pump process, atoms at different positions might experience different shifts, which leads to an effective inhomogeneous broadening of the ensemble. But as long as the frequency distribution is small enough, the atoms can still synchronize and emit light collectively on a single narrow line [7,15,30]. For an ensemble with an inhomogeneous frequency broadening less than the incoherent pump rate R the atoms synchronize in the superradiant regime. Note that the incoherent pumping reduces the coherence between the atoms, thus there is also an upper bound of $R + \nu < 4Ng^2/\kappa$ [4,8,15] for the repumping rate.

Our aim is therefore to find parameters with an effective repumping rate $R > 2\pi \cdot 1$ Hz, but also sufficiently small frequency shift changes of the clock transition for realistic fluctuations and inaccuracies in the pump process. To this end we scan the effective repumping rate R and the

Optics EXPRESS

ground state shift δ_1 on the relevant system parameters. Note that we only get shifts of the lower clock state in our model, since no pump laser couples to the upper clock state.

A parameter set to achieve the above goal is: $\Omega_{13} = 2\pi \cdot 1.5$ kHz, $\Omega_{34} = 2\pi \cdot 3.3$ MHz, $\Omega_{54} = 2\pi \cdot 100$ kHz, $\Delta_{13} = -2\pi \cdot 875$ kHz, $\Delta_{34} = -2\pi \cdot 5$ MHz and $\Delta_{54} = -2\pi \cdot 10$ MHz. The corresponding two-level system parameters are $R \approx 2\pi \cdot 1.91$ Hz, $\delta_1 \approx 2\pi \cdot 5.21$ mHz and $\nu \approx 2\pi \cdot 3.93$ Hz. These results are for pump laser linewidth of $\nu_{13} = \nu_{34} = \nu_{54} = 2\pi \cdot 0.75$ kHz and a dephasing rate on the clock transition of $\nu = 2\pi \cdot 1$ Hz. We will use these parameters as our "standard" parameters, i.e. whenever parameters are kept constant in scans we use these.

Figure 2 shows the dependence of the effective repumping rate R and the ground state shift δ_1 on the Rabi-frequencies Ω_{13} and Ω_{34} (upper row) as well as on the detunings Δ_{13} and Δ_{34} (lower row), when the other parameters are kept constant. We do not show here scans on Δ_{54} and Ω_{54}, since the dependences of R and δ_1 are very weak over a wide range of parameters, see one-dimensional scans in appendix B. One can also see from these scans, that the dependence of both, R and δ_1, on Ω_{13} is quadratic. Therefore, the sensitivity of δ_1 to variations of Ω_{13} is proportional to δ_1, which means one should choose a working point with δ_1 close to zero (dark blue regions in Fig. 2(b) and (e)), otherwise rather small fluctuations on Ω_{13} might lead to big variations of δ_1.

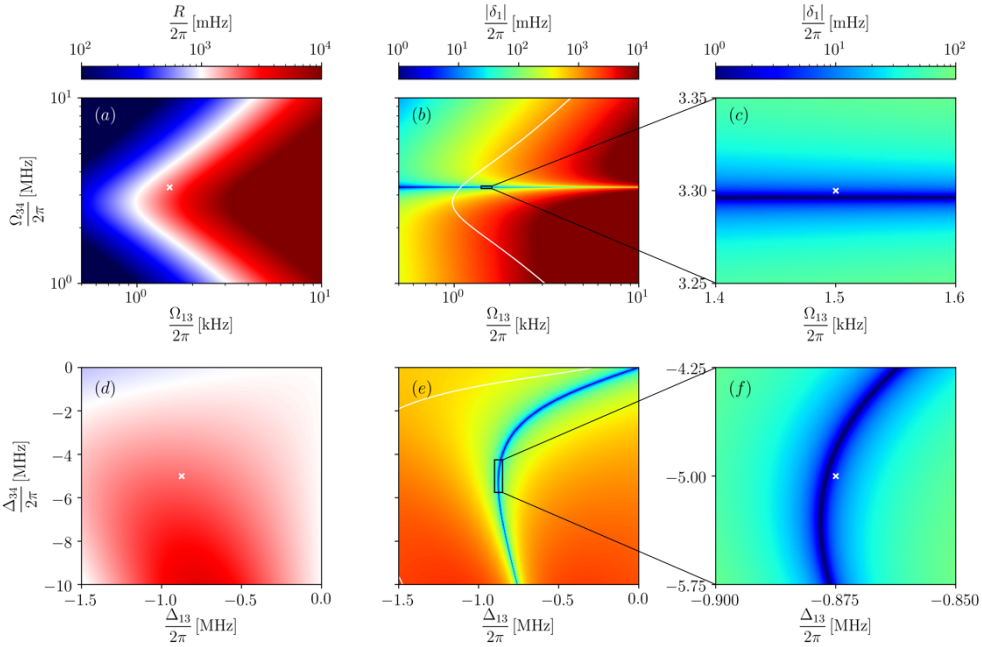

Fig. 2. *Parameter scans of the effective pump rate R and the differential shift of the lasing transition* δ_1. In the upper row (a-c) we vary the amplitudes of the two pump lasers and in the lower row (d-f) their frequency detuning. We are targeting regions of sufficiently high pump rate and very low shift. The white contour line in the $|\delta_1|$-scans depicts $R = 2\pi \cdot 1$ Hz. Figure (c) and (f) show a zoom in a parameter region with small shifts $|\delta_1| < 2\pi \cdot 100$ mHz. The white crosses indicate the parameters fixed in the other plots.

From the subplots (a) and (d) of Fig. 2 we can see, that there are wide regions with an effective repumping rate $R > 2\pi \cdot 1$ Hz. In the subplots (b) and (e) we plot the ground state shift and additionally indicate the relevant regions with a white line, which shows the repumping of $R = 2\pi \cdot 1$ Hz. In the panel (c) we zoom into an appropriate region for the Rabi-frequency scan.

Optics EXPRESS

We see that for our parameters a deviation in Ω_{34} of $\pm 1.5\%$ still has tolerable shifts. For Ω_{13} the suitable range is much bigger.

In the panel (f) we show a proper region for the detuning scan. We chose an area with a suitable range for Δ_{13} of $2\pi \cdot 50$ kHz and for Δ_{34} of $2\pi \cdot 1.5$ MHz. The reason to pick this region is the following: To avoid Doppler shifts a magic wavelength optical lattice is needed to trap the strontium atoms, but this lattice is in general only magic on the clock transition. This means for the other transitions the upper and lower state are not equally shifted and therefore non-clock transitions of atoms at different positions in the lattice have shifted resonance frequencies. However, the lattice can also be made magic on the $|1\rangle \leftrightarrow |3\rangle$ transition for a linearly polarized field, if one chooses the correct angle between the polarization axis and the quantization axis due to the static magnetic field [46]. Nonetheless, this does not work simultaneously on the $|3\rangle \leftrightarrow |4\rangle$ transition, which results in an effective inhomogeneous broadening of the transition frequency ω_{34} and hence in a Δ_{34} distribution. According to recent theoretical estimations [47], the scalar and tensor dynamic polarizabilities of the $(5s6s)^3S_1$ state at the 813 nm magic wavelength lattice are $\alpha_0(^3S_1) \approx -9 \times 10^2$ a.u. (atomic units) and $\alpha_2(^3S_1) \approx 2$ a.u., respectively. In turn, the scalar polarizabilities of the lasing states $|1\rangle$ and $|2\rangle$ at the magic wavelength are equal to $a_0(^1S_0) = a_0(^3P_0) \approx 2.8 \times 10^2$ a.u. [48]. A thermal distribution of the atoms over different vibrational states and/or lattice sites with different potential depths will results into different shifts of the level $|4\rangle$. In particular, a temperature of $T = 5$ µK corresponds to a shift of level $|4\rangle$ in the range of approximately 0.4 MHz, which directly results in a Δ_{34} distribution. Therefore we need to choose parameters with a wide suitable range for Δ_{34}, but we can pick a point with a rather narrow range for Δ_{13}.

In summary, the main result in this section is that it occurs to be possible to achieve a significant repumping rate R together with a sufficient small and insensitive shift δ_1. The optimal set of parameters will be individual for each experimental setup, but they can be found fast with the above described method.

4. Effective linewidth and shift in the reduced laser model

In this section we calculate the spectrum of the superradiant laser, and demonstrate that our six-level laser model can be replaced by an effective two-level one. The laser model is given by N identical six-level atoms pumped inside an optical cavity. In the rotating frame of the pump lasers and the unperturbed clock transition the Hamiltonian can be written as

$$\begin{aligned} H_{\mathrm{L6}} = &-\Delta_c a^\dagger a + \sum_{k=1}^{N} \Big[-\Delta_3 \hat{\sigma}_{33}^k - \Delta_4 \hat{\sigma}_{44}^k - \Delta_5 \hat{\sigma}_{55}^k + g(a^\dagger \hat{\sigma}_{12}^k + a\hat{\sigma}_{21}^k) \\ &+\Omega_{13}(\hat{\sigma}_{13}^k + \hat{\sigma}_{31}^k) + \Omega_{34}(\hat{\sigma}_{34}^k + \hat{\sigma}_{43}^k) + \Omega_{54}(\hat{\sigma}_{45}^k + \hat{\sigma}_{54}^k)\Big]. \end{aligned} \tag{12}$$

Here $\Delta_c = \omega_{12} - \omega_c$ is the detuning between the clock transition frequency and the cavity resonance frequency, and g is the coupling coefficient between the cavity field and the clock transition. The dissipative processes for the atoms are listed in Table 2. The dissipative processes of the cavity are according to Table 3. Using that all atoms behave identically we derive second order cumulant equations [40,41] for the system variables and the correlation function [49]. However, we can use the adiabatic elimination from section 2 to numerically reduce the six-level atom lasing model into an effective two-level atom lasing model. This simplifies the model drastically and increases the computational efficiency significantly. The Hamiltonian of this two-level lasing model is

$$H_{\mathrm{L2}} = -\Delta_c a^\dagger a + \sum_{k=1}^{N} \Big[-\delta_1^k \hat{\sigma}_{22}^k + g_k(a^\dagger \hat{\sigma}_{12}^k + a\hat{\sigma}_{21}^k)\Big] \tag{13}$$

Optics EXPRESS

and the dissipative processes are given by Table 3 for the cavity and Table 1 for each of the N atoms individually.

Table 3. Dissipative processes of the cavity field.

#	jump	rate	description
1	a	κ	cavity photon losses
2	$a^\dagger a$	η	fluctuations of the cavity resonance frequency

In Fig. 3 we see the excellent agreement of the laser properties calculated from the effective two-level lasing model and the six-level model for our standard parameters. We compared these two models for many other relevant parameters, the laser properties (FWHM, δ_p, $\langle a^\dagger a\rangle$) always agreed well. Furthermore, Fig. 3 indicates that a cavity dephasing up to $\eta = \kappa/10$ does not significantly influence the spectrum, as expected for a superradiant laser. A comparison with the case of no cavity dephasing ($\eta = 0$) showed essentially the same laser properties.

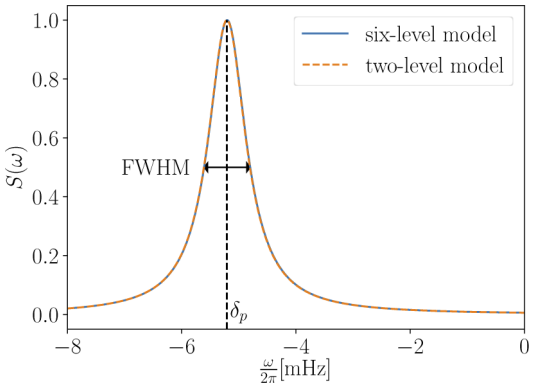

Fig. 3. *Laser spectrum.* Comparison of the the effective two-level model with the full six-level model for a typical set of parameters. The laser properties are FWHM = $2\pi\cdot 0.806$ mHz ($2\pi\cdot 0.807$ mHz for the six-level model), $\delta_p = -2\pi\cdot 5.20$ mHz ($-2\pi\cdot 5.21$ mHz) and an intra-cavity photon number of $\langle a^\dagger a\rangle = 2.16\,(2.15)$, with an inaccuracy of the effective model below 1%. The atom number is $N = 2\cdot 10^5$ and the cavity parameters are $\kappa = 2\pi\cdot 75$ kHz, $g = 2\pi\cdot 2$ Hz and $\eta = 2\pi\cdot 7.5$ kHz.

Finally, let us discuss the effect of the pump laser induced dephasing. The main mechanism of such a dephasing is that the atoms pumped into the upper states $|3\rangle$ and $|4\rangle$ can decay into the state $|1\rangle$, instead of into the upper lasing state $|2\rangle$, see also appendix A. Therefore, the dephasing rate ν needs to be proportional to the effective incoherent repumping rate R. Since the only way to get into the state $|2\rangle$ is to decay from $|4\rangle$ and since all other transitions are driven, the most prominent process to end up in $|1\rangle$ is via the decay into $|6\rangle$, therefore we can estimate

$$\nu \approx R\frac{\Gamma_{64}}{\Gamma_{24}} + \nu_{12} \approx 1.5R + \nu_{12}. \tag{14}$$

For the parameters used in Fig. 3 we get a FWHM of $\sim 2\pi\cdot 0.81$ mHz. In comparison the smallest linewidth we could theoretically get is $4g^2/\kappa \approx 2\pi\cdot 0.21$ mHz. With no dephasing at all ($\nu = 0$) this can, for these parameters, indeed be reached. Thus we see that the induced dephasing has an impact on the spectrum which is not to be neglected, but it is still reasonable. Note that the induced dephasing could e.g. be decreased in our case by additionally pumping the transition $|4\rangle \leftrightarrow |6\rangle$.

Optics EXPRESS

5. Conclusions

On the example of bosonic strontium trapped in a magic wavelength optical lattice we show that by choice of suitable pump laser parameters, it is possible to create significant population inversion on the clock transition with only a rather small shift and broadening of the lasing transition and the resulting active clock line. In particular we found a parameter regime where the induced level shifts on the clock transition are small enough, such that the atoms can still synchronize and thus emit light collectively in the superradiant regime, where cavity noise plays no role. To perform our scans of the many parameters characterizing the complex multilevel system, we have developed a fast numerical way to map the results to an effective two-level model, which can be well interpreted. For a range of generic test cases we have seen that the spectral and noise properties of these two models are in excellent agreement. The procedure can be adapted straight forward to find suitable repumping parameter for ^{88}Sr in a weaker magnetic field as well as for fermionic ^{87}Sr and other alkaline-earth atoms. The possibility to simultaneously cool the atoms has been briefly mentioned, a further detailed investigation of this is planed to be done in the future.

Appendix A. Analytic adiabatic elimination on a three-level atom

Here we compare the "conventional" adiabatic elimination with the adiabatic elimination using the eigenvalues of the non-hermitian Hamiltonian. We apply the two methods analytically on a pumped three-level atom to eliminate the auxiliary level $|3\rangle$.

The atom is coherently pumped on the transition $|1\rangle \leftrightarrow |3\rangle$ with a Rabi frequency Ω and laser detuning Δ_3, see Fig. 4. We suppose that the Rabi frequency Ω as well as the decay and decoherence rates associated with the state $|3\rangle$ (Γ_{13}, Γ_{23}, ν_3) are much larger than all the other rates in the system, and that the total decay rate of level $|3\rangle$ is much larger than Ω, therefore the population of the level $|3\rangle$ is much less than the populations of the levels $|1\rangle$ and $|2\rangle$. The Hamiltonian of a single atom can be written as

$$\hat{H} = \hbar(\Delta_2\hat{\sigma}_{22} + \Delta_3\hat{\sigma}_{33}) + \hbar\Omega(\hat{\sigma}_{13} + \hat{\sigma}_{31}), \tag{15}$$

where Δ_2 is some shift from the unperturbed atomic transition frequency. Jump operators and relaxation rates are listed in Table 4. Note that we neglect the interaction with the weak cavity field, see section 2.

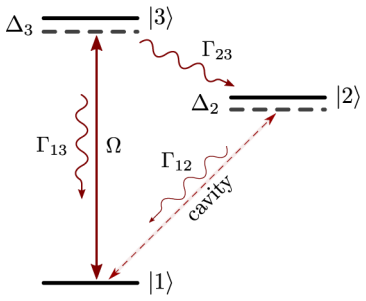

Fig. 4. *Three-level scheme.* The considered three-level scheme for the adiabatic elimination of level $|3\rangle$ is depicted. The atoms are coherently pumped on the transition $|1\rangle \leftrightarrow |3\rangle$ and the cavity couples on the transition $|1\rangle \leftrightarrow |2\rangle$.

A.1. "Conventional" adiabatic elimination

First we perform an adiabatic elimination of the level $|3\rangle$, in the "conventional" way, similar to the one used in [16]. To this end we calculate the relevant equations for operator averages $\langle\hat{\sigma}_{\alpha,\beta}\rangle$,

Optics EXPRESS

Table 4. Dissipative processes of the three-level atom.

#	jump	rate	description
1	$\hat{\sigma}_{12}$	Γ_{12}	decay from $\|2\rangle$ to $\|1\rangle$
2	$\hat{\sigma}_{13}$	Γ_{13}	decay from $\|3\rangle$ to $\|1\rangle$
3	$\hat{\sigma}_{23}$	Γ_{23}	decay from $\|3\rangle$ to $\|2\rangle$
4	$\hat{\sigma}_{11}$	ν_1^0	dephasing on $\|1\rangle$
5	$\hat{\sigma}_{22}$	ν_2^0	dephasing on $\|2\rangle$
6	$\hat{\sigma}_{33}$	ν_3^0	dephasing on $\|3\rangle$

where $\alpha, \beta \in \{1, 2, 3\}$:

$$\frac{d\langle\hat{\sigma}_{22}\rangle}{dt} = -\Gamma_{12}\langle\hat{\sigma}_{22}\rangle + \Gamma_{23}\langle\hat{\sigma}_{33}\rangle \tag{16}$$

$$\frac{d\langle\hat{\sigma}_{12}\rangle}{dt} = -\left(\frac{\Gamma_{12} + \nu_1^0 + \nu_2^0}{2} + i\Delta_2\right)\langle\hat{\sigma}_{12}\rangle + i\Omega\langle\hat{\sigma}_{32}\rangle \tag{17}$$

$$\frac{d\langle\hat{\sigma}_{33}\rangle}{dt} = i\Omega\langle\hat{\sigma}_{13} - \hat{\sigma}_{31}\rangle - \Gamma_3\langle\hat{\sigma}_{33}\rangle \tag{18}$$

$$\frac{d\langle\hat{\sigma}_{13}\rangle}{dt} = -\left(\frac{\Gamma_3 + \nu_1^0 + \nu_3^0}{2} + i\Delta_3\right)\langle\hat{\sigma}_{13}\rangle - i\Omega\langle\hat{\sigma}_{11} - \hat{\sigma}_{33}\rangle \tag{19}$$

$$\frac{d\langle\hat{\sigma}_{23}\rangle}{dt} = -\left(\frac{\Gamma_3 + \Gamma_{12} + \nu_2^0 + \nu_3^0}{2} + i\Delta_3\right)\langle\hat{\sigma}_{23}\rangle - i\Omega\langle\hat{\sigma}_{21}\rangle \tag{20}$$

Here $\Gamma_3 = \Gamma_{13} + \Gamma_{23}$ is the total decay rate of the intermediate state $|3\rangle$. To perform the adiabatic elimination of $\langle\hat{\sigma}_{33}\rangle$, $\langle\hat{\sigma}_{23}\rangle$, $\langle\hat{\sigma}_{13}\rangle$ we use $\Gamma_{12} \ll \Gamma_3$ and $\nu_1^0, \nu_2^0 \ll \nu_3^0$ as well as $\langle\hat{\sigma}_{33}\rangle \ll \langle\hat{\sigma}_{11}\rangle$. Introducing

$$\Gamma' = \frac{\Gamma_3 + \nu_3^0}{2} \approx \frac{\Gamma_3 + \Gamma_{12} + \nu_2^0 + \nu_3^0}{2} \approx \frac{\Gamma_3 + \nu_1^0 + \nu_3^0}{2} \tag{21}$$

we get

$$\langle\hat{\sigma}_{13}\rangle = \frac{-i\Omega}{\Gamma' + i\Delta_3}\langle\hat{\sigma}_{11}\rangle \tag{22}$$

$$\langle\hat{\sigma}_{23}\rangle = \frac{-i\Omega}{\Gamma' + i\Delta_3}\langle\hat{\sigma}_{21}\rangle \tag{23}$$

$$\langle\hat{\sigma}_{33}\rangle = \frac{2\Omega^2}{\Gamma_3}\frac{\Gamma'}{\Gamma'^2 + {\Delta_3}^2}\langle\hat{\sigma}_{11}\rangle. \tag{24}$$

Substituting these expressions into (16) – (17), and introducing the repumping rate R, decoherence rate ν_{12} and effective shift Δ_{21} as

$$R = \frac{\Gamma_{23}}{\Gamma_3}\frac{2\Omega^2\Gamma'}{\Gamma'^2 + {\Delta_3}^2} \tag{25}$$

$$\nu_{12} = \nu_1^0 + \nu_2^0 + \frac{\Gamma_{13}}{\Gamma_3}\frac{2\Omega^2\Gamma'}{\Gamma'^2 + {\Delta_3}^2} \tag{26}$$

$$\Delta_{21} = \Delta_2 + \frac{\Omega^2\Delta_3}{\Gamma'^2 + {\Delta_3}^2} \tag{27}$$

Optics EXPRESS

we can rewrite the Eqs. (16) and (17) as

$$\frac{d\langle\hat{\sigma}_{22}\rangle}{dt} = -\Gamma_{12}\langle\hat{\sigma}_{22}\rangle + R\langle\hat{\sigma}_{11}\rangle \tag{28}$$

$$\frac{d\langle\hat{\sigma}_{12}\rangle}{dt} = -\left(\frac{R+\Gamma_{12}+\nu_{12}}{2} + i\Delta_{21}\right)\langle\hat{\sigma}_{12}\rangle, \tag{29}$$

similar to Eqs. (3) and (4).

A.2. Adiabatic elimination using the eigenvalues of the non-hermitian Hamiltonian

Now we apply the procedure described in the end of Section 2. The simplicity of the considered 3-level scheme allows to follow this method analytically. The expression for the repumping rate R, see Eq. (5), can be obtained from the steady-state expression of $\langle\hat{\sigma}_{22}\rangle$ and $\langle\hat{\sigma}_{33}\rangle$,

$$\langle\hat{\sigma}_{22}\rangle = \frac{\Gamma_{23}}{\Gamma_{12}}\langle\hat{\sigma}_{33}\rangle = \frac{\Gamma_{23}}{\Gamma_{12}}\frac{2\Omega^2\Gamma'}{\Gamma(\Gamma'^2+{\Delta_3}^2)}\langle\hat{\sigma}_{11}\rangle. \tag{30}$$

The result is the same as in (25).

To determine the light shift and decoherence rate, one has to diagonalize the effective non-Hermitian Hamiltonian of our 3-level system in the absence of the cavity field. The Hamiltonian reads

$$\begin{aligned}\hat{H}_{\text{eff}}^{\text{nh}} &= \hat{H} - \frac{i\hbar}{2}\sum_j R_j\hat{J}_j^\dagger\hat{J}_j \\ &= \hbar(\delta_2\hat{\sigma}_{22} + \Delta_3\hat{\sigma}_{33} + \Omega[\hat{\sigma}_{13}+\hat{\sigma}_{31}]) - \frac{i\hbar}{2}\left[\Gamma_{12}\hat{\sigma}_{22} + \Gamma\hat{\sigma}_{33} + \nu_1^0\hat{\sigma}_{11} + \nu_2^0\hat{\sigma}_{22} + \nu_3^0\hat{\sigma}_{33})\right]\end{aligned} \tag{31}$$

with the eigenvalues

$$\frac{E_2}{\hbar} = \Delta_2 - \frac{i}{2}(\Gamma_{12}+\nu_2^0) \tag{32}$$

$$\frac{E_{1,3}}{\hbar} = \frac{\Delta_3 - i\Gamma'}{2}\left\{1 \mp \sqrt{1 + \frac{4\Omega^2 + 2i\nu_1^0(\Delta_3 - i\Gamma')}{(\Delta_3 - i\Gamma')^2}}\right\}, \tag{33}$$

where Γ' is defined in (21), and we neglected Γ_{12}, ν_1^0 and ν_2^0 in comparison with Γ'. For $\nu_1^0, \Omega \ll \Gamma'$ we can perform a Taylor expansion on the term $[4\Omega^2 + 2i\nu_1^0(\Delta_3 - i\Gamma')]/(\Delta_3 - i\Gamma')^2 \ll 1$ and find

$$\frac{E_1}{\hbar} \approx -\frac{\Omega^2(\Delta_3 + i\Gamma')}{{\Delta_3}^2 + \Gamma'^2} - \frac{i\nu_1^0}{2}. \tag{34}$$

Using expressions (10), we get

$$\Delta_1 = -\frac{\Omega^2\Delta_3}{\Gamma'^2 + {\Delta_3}^2} \tag{35}$$

$$\nu_1 = \nu_1^0 + \frac{2\Gamma'\Omega^2}{\Gamma'^2+{\Delta_3}^2} - R = \nu_1^0 + \frac{\Gamma_{13}}{\Gamma}\frac{2\Omega^2\Gamma'}{\Gamma'^2+{\Delta_3}^2}. \tag{36}$$

Similarly, from (32) follows $\nu_2 = \nu_2^0$. Therefore we obtain

$$\nu_{12} = \nu_1 + \nu_2 = \nu_1^0 + \nu_2^0 + \frac{\Gamma_{13}}{\Gamma}\frac{2\Omega^2\Gamma'}{\Gamma'^2+{\Delta_3}^2} \tag{37}$$

Optics EXPRESS

$$\Delta_{21} = \Delta_2 - \Delta_1 = \Delta_2 + \frac{\Omega^2 \Delta_3}{\Gamma'^2 + {\Delta_3}^2}, \tag{38}$$

this coincides with (26) and (27). Thus, we can see that th adiabatic elimination in such a 3-level system performed with the help of the diagonalization of the effective non-Hermitian Hamiltonian gives the same result as a "conventional" adiabatic elimination.

Appendix B. One dimensional parameter scans

To get a better insight of the dependence on the different repumping parameters we show here one dimensional scans. Figure 5 shows scans on the Rabi-frequencies and Fig. 6 on the detunings for R and δ_1. The scans on Ω_{13}, Fig. 5(a) and (d), show a quadratic dependence of R and δ_1 on the relevant regions of Ω_{13} with a constant prefactor depending on the other system parameters. A proper choice of parameters can reduce the prefactor of the ground state shift by orders of magnitudes, while the pump rate prefactor stays almost the same. For the Ω_{34}-scans, Fig. 5(b) and (e), we find only a relative small area at approximately $\Omega_{34} \approx 2\pi \cdot 3.3$ MHz (see inset) where a repumping rate $R > 2\pi \cdot 1$ Hz can be achieved and the range of the shift $|\delta_1|$ is sufficiently small. For Ω_{54}, Fig. 5(c) and (f), on the other hand, all values below $2\pi \cdot 1$ MHz have an almost constant R and δ_1. But note that for smaller values of Ω_{54} more population is trapped in $|5\rangle$, this is undesired since less population will contribute to lasing. However, for our parameters this gets only relevant for $\Omega_{54} < 2\pi \cdot 1$ kHz.

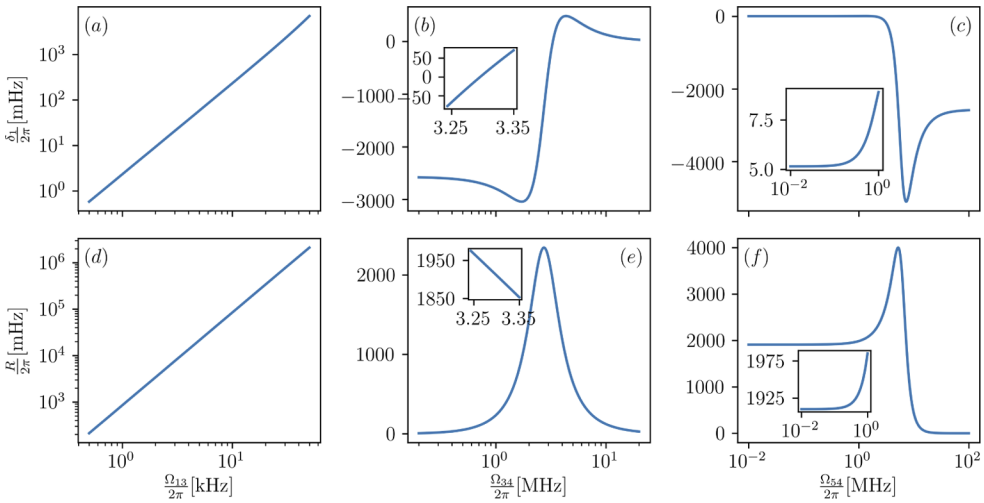

Fig. 5. *Line shift (upper row) and pump rate (lower row) scans for varying pump amplitudes close to optimal operation conditions*. The dependence of the ground state shift and the repumping rate on the Rabi frequencies is shown with insets of interesting regions. The parameters when kept constant are our standard parameters from section 3.1.

As we know from section 3.1 Δ_{13} can be controlled much more precisely than Δ_{34} due to the magic wavelength lattice, therefore we choose a parameter regime in which changes of Δ_{34} are far less important. Figure 6 illustrates this very well. Differences in Δ_{13} of $\pm 2\pi \cdot 25$ kHz lead to shifts of $\pm 2\pi \cdot 50$ mHz, whereas changes of $\pm 2\pi \cdot 0.75$ MHz in Δ_{34} lead only to shifts in a range of approximately $2\pi \cdot 40$ mHz, see Fig. 6(a) and (b) respectively. For the Δ_{54} dependency, Fig. 6(c) and (f), we find that R and δ_1 do not significantly change for detunings between $-2\pi \cdot 15$ and $-2\pi \cdot 6$ MHz. Thus Δ_{54} does not need to be precisely controlled.

Optics EXPRESS

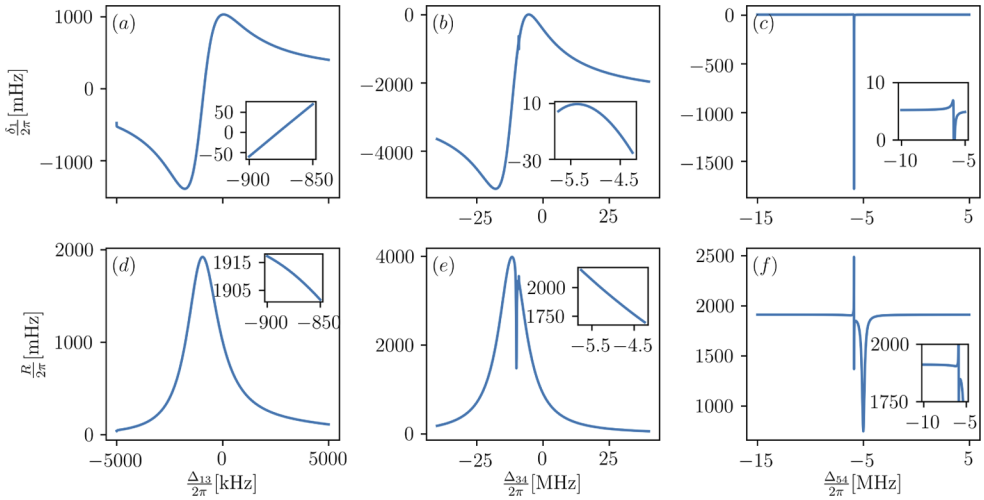

Fig. 6. *Line shift (upper row) and pump rate (lower row) scans for varying pump detunings close to optimal operation conditions*. The dependence of the ground state shift and the repumping rate on the detunings is shown with insets of interesting regions. The parameters when kept constant are our standard parameters from section 3.1.

Funding. Horizon 2020 Framework Programme (820404).

Acknowledgment. This work was supported by the European Union Horizon 2020 research and innovation programme, Quantum Flagship project No 820404 "iqClock" (C. H., D. P., G.K. and H. R.). Numerical simulations were performed with the open source frameworks QuantumOptics.jl [50] and QuantumCumulants.jl [41]. The graphs were produced using the open source plotting library Matplotlib [51]. The authors thank Marianna Safronova and Dmytro Filin for calculations of the dynamic polarizabilities on the $^3S_1$ state in neutral strontium atoms.

Disclosures. The authors declare no conflicts of interest.

Data availability. Programs to simulate the physical models are available in Code 1, Ref. [52]; Code 2, Ref. [53]; and Code 3, Ref. [54]. Data underlying the results presented in this paper are not publicly available at this time but may be obtained from the authors upon reasonable request.

References

1. E. Oelker, R. Hutson, C. Kennedy, L. Sonderhouse, T. Bothwell, A. Goban, D. Kedar, C. Sanner, J. Robinson, G. Marti, D. Matei, T. Legero, M. Giunta, R. Holzwarth, F. Riehle, U. Sterr, and J. Ye, "Demonstration of 4.8× 10- 17 stability at 1 s for two independent optical clocks," Nat. Photonics **13**(10), 714–719 (2019).
2. K. Numata, A. Kemery, and J. Camp, "Thermal-noise limit in the frequency stabilization of lasers with rigid cavities," Phys. Rev. Lett. **93**(25), 250602 (2004).
3. J. Chen, "Active optical clock," Chin. Sci. Bull. **54**(3), 348–352 (2009).
4. D. Meiser, J. Ye, D. Carlson, and M. Holland, "Prospects for a millihertz-linewidth laser," Phys. Rev. Lett. **102**(16), 163601 (2009).
5. J. G. Bohnet, Z. Chen, J. M. Weiner, D. Meiser, M. J. Holland, and J. K. Thompson, "A steady-state superradiant laser with less than one intracavity photon," Nature **484**(7392), 78–81 (2012).
6. J. G. Bohnet, Z. Chen, J. M. Weiner, K. C. Cox, and J. K. Thompson, "Linear-response theory for superradiant lasers," Phys. Rev. A **89**(1), 013806 (2014).
7. A. Bychek, C. Hotter, D. Plankensteiner, and H. Ritsch, "Superradiant lasing in inhomogeneously broadened ensembles with spatially varying coupling," Open Res. Europe **1**, 73 (2021).
8. K. Debnath, Y. Zhang, and K. Mølmer, "Lasing in the superradiant crossover regime," Phys. Rev. A **98**(6), 063837 (2018).
9. A. Gogyan, G. Kazakov, M. Bober, and M. Zawada, "Characterisation and feasibility study for superradiant lasing in 40ca atoms," Opt. Express **28**(5), 6881–6892 (2020).
10. F. Haake, M. I. Kolobov, C. Fabre, E. Giacobino, and S. Reynaud, "Superradiant laser," Phys. Rev. Lett. **71**(7), 995–998 (1993).
11. C. Hotter, D. Plankensteiner, L. Ostermann, and H. Ritsch, "Superradiant cooling, trapping, and lasing of dipole-interacting clock atoms," Opt. Express **27**(22), 31193–31206 (2019).

Optics EXPRESS

12. S. B. Jäger, H. Liu, A. Shankar, J. Cooper, and M. J. Holland, "Regular and bistable steady-state superradiant phases of an atomic beam traversing an optical cavity," Phys. Rev. A **103**(1), 013720 (2021).
13. G. A. Kazakov and T. Schumm, "Active optical frequency standard using sequential coupling of atomic ensembles," Phys. Rev. A **87**(1), 013821 (2013).
14. G. A. Kazakov and T. Schumm, "Active optical frequency standards using cold atoms: perspectives and challenges," in *2014 European Frequency and Time Forum (EFTF)*, (IEEE, 2014), pp. 411–414.
15. G. A. Kazakov and T. Schumm, "Stability analysis for bad cavity lasers using inhomogeneously broadened spin-1/2 atoms as a gain medium," Phys. Rev. A **95**(2), 023839 (2017).
16. G. A. Kazakov, J. Bohnet, and T. Schumm, "Prospects for a bad-cavity laser using a large ion crystal," Phys. Rev. A **96**(2), 023412 (2017).
17. T. Laske, H. Winter, and A. Hemmerich, "Pulse delay time statistics in a superradiant laser with calcium atoms," Phys. Rev. Lett. **123**(10), 103601 (2019).
18. H. Liu, S. B. Jäger, X. Yu, S. Touzard, A. Shankar, M. J. Holland, and T. L. Nicholson, "Rugged mhz-linewidth superradiant laser driven by a hot atomic beam," Phys. Rev. Lett. **125**(25), 253602 (2020).
19. T. Maier, S. Kraemer, L. Ostermann, and H. Ritsch, "A superradiant clock laser on a magic wavelength optical lattice," Opt. Express **22**(11), 13269–13279 (2014).
20. D. Meiser and M. Holland, "Intensity fluctuations in steady-state superradiance," Phys. Rev. A **81**(6), 063827 (2010).
21. D. Meiser and M. Holland, "Steady-state superradiance with alkaline-earth-metal atoms," Phys. Rev. A **81**(3), 033847 (2010).
22. M. A. Norcia and J. K. Thompson, "Cold-strontium laser in the superradiant crossover regime," Phys. Rev. X **6**(1), 011025 (2016).
23. M. A. Norcia, M. N. Winchester, J. R. Cline, and J. K. Thompson, "Superradiance on the millihertz linewidth strontium clock transition," Sci. Adv. **2**(10), e1601231 (2016).
24. M. A. Norcia, R. J. Lewis-Swan, J. R. Cline, B. Zhu, A. M. Rey, and J. K. Thompson, "Cavity-mediated collective spin-exchange interactions in a strontium superradiant laser," Science **361**(6399), 259–262 (2018).
25. M. A. Norcia, J. R. Cline, J. A. Muniz, J. M. Robinson, R. B. Hutson, A. Goban, G. E. Marti, J. Ye, and J. K. Thompson, "Frequency measurements of superradiance from the strontium clock transition," Phys. Rev. X **8**(2), 021036 (2018).
26. S. A. Schäffer, M. Tang, M. R. Henriksen, A. A. Jørgensen, B. T. Christensen, and J. W. Thomsen, "Lasing on a narrow transition in a cold thermal strontium ensemble," Phys. Rev. A **101**(1), 013819 (2020).
27. M. Tang, S. A. Schäffer, A. A. Jørgensen, M. R. Henriksen, B. T. Christensen, J. H. Müller, and J. W. Thomsen, "Cavity-immune spectral features in the pulsed superradiant crossover regime," Phys. Rev. Res. **3**(3), 033258 (2021).
28. A. Shankar, J. T. Reilly, S. B. Jäger, and M. J. Holland, "Subradiant-to-subradiant phase transition in the bad cavity laser," Phys. Rev. Lett. **127**, 073603 (2021).
29. J. M. Weiner, K. C. Cox, J. G. Bohnet, and J. K. Thompson, "Phase synchronization inside a superradiant laser," Phys. Rev. A **95**(3), 033808 (2017).
30. M. Xu, D. A. Tieri, E. Fine, J. K. Thompson, and M. J. Holland, "Synchronization of two ensembles of atoms," Phys. Rev. Lett. **113**(15), 154101 (2014).
31. Y. Zhang, C. Shan, and K. Mølmer, "Ultranarrow superradiant lasing by dark atom-photon dressed states," Phys. Rev. Lett. **126**(12), 123602 (2021).
32. H. M. Goldenberg, D. Kleppner, and N. F. Ramsey, "Atomic hydrogen maser," Phys. Rev. Lett. **5**(8), 361–362 (1960).
33. V. S. Strelnitski, V. O. Ponomarev, and H. A. Smith, "Hydrogen masers. i: Theory and prospects," arXiv preprint astro-ph/9511118 (1995).
34. T. Salzburger and H. Ritsch, "Atom-photon pair laser," Phys. Rev. A **75**(6), 061601 (2007).
35. C.-C. Chen, S. Bennetts, R. G. Escudero, B. Pasquiou, and F. Schreck, "Continuous guided strontium beam with high phase-space density," Phys. Rev. Appl. **12**(4), 044014 (2019).
36. H. Katori, M. Takamoto, V. Pa'Chikov, and V. Ovsiannikov, "Ultrastable optical clock with neutral atoms in an engineered light shift trap," Phys. Rev. Lett. **91**(17), 173005 (2003).
37. J. Ye, H. Kimble, and H. Katori, "Quantum state engineering and precision metrology using state-insensitive light traps," Science **320**(5884), 1734–1738 (2008).
38. R. G. Escudero, C.-C. Chen, S. Bennetts, B. Pasquiou, and F. Schreck, "A steady-state magneto-optical trap of fermionic strontium on a narrow-line transition," arXiv preprint arXiv:2104.06814 (2021).
39. S. Bennetts, C.-C. Chen, B. Pasquiou, and F. Schreck, "Steady-state magneto-optical trap with 100-fold improved phase-space density," Phys. Rev. Lett. **119**(22), 223202 (2017).
40. R. Kubo, "Generalized cumulant expansion method," J. Phys. Soc. Jpn. **17**(7), 1100–1120 (1962).
41. D. Plankensteiner, C. Hotter, and H. Ritsch, "QuantumCumulants.jl: A Julia framework for generalized mean-field equations in open quantum systems," Quantum **6**, 617 (2022).
42. R. Dum, P. Zoller, and H. Ritsch, "Monte carlo simulation of the atomic master equation for spontaneous emission," Phys. Rev. A **45**(7), 4879–4887 (1992).
43. K. Mølmer, Y. Castin, and J. Dalibard, "Monte carlo wave-function method in quantum optics," J. Opt. Soc. Am. B **10**(3), 524–538 (1993).
44. M. B. Plenio and P. L. Knight, "The quantum-jump approach to dissipative dynamics in quantum optics," Rev. Mod. Phys. **70**(1), 101–144 (1998).

Optics EXPRESS

45. A. Kramida, Y. Ralchenko, J. Reader, and NIST ASD Team, "NIST Atomic Spectra Database (ver. 5.8)," National Institute of Standards and Technology (2020) [Online]. Available: https://physics.nist.gov/asd [2021, September 1].
46. D. S. Barker, N. C. Pisenti, B. J. Reschovsky, and G. K. Campbell, "Three-photon process for producing a degenerate gas of metastable alkaline-earth-metal atoms," Phys. Rev. A **93**(5), 053417 (2016).
47. D. Filin and M. Safronova, "private communication," (2021).
48. M. J. Martin, "Quantum metrology and many-body physics: Pushing the frontier of the optical lattice clock," Ph.D. thesis, University of Colorado (2013).
49. Program examples using the Julia package QuantumCumulants.jl, which analytically derive the system and correlation function equations for the six-level and two-level laser model are given in the supplementary material. Additionaly we show an example to calculate the two-level system parameters from the pumped six-level atom, using the Julia package QuantumOptics.jl. The equations in these examples are solved numerically for our standard parameters.
50. S. Krämer, D. Plankensteiner, L. Ostermann, and H. Ritsch, "QuantumOptics.jl: A Julia framework for simulating open quantum systems," Comput. Phys. Commun. **227**, 109–116 (2018).
51. J. D. Hunter, "Matplotlib: A 2d graphics environment," Comput. Sci. Eng. **9**(3), 90–95 (2007).
52. C. Hotter, D. Plankensteiner, G. Kazakov, and H. Ritsch, "Code 1: 2-level atom laser example program," figshare (2022), https://doi.org/10.6084/m9.figshare.18095849.
53. C. Hotter, D. Plankensteiner, G. Kazakov, and H. Ritsch, "Code 2: 6-level atom laser example program," figshare (2022), https://doi.org/10.6084/m9.figshare.18095852.
54. C. Hotter, D. Plankensteiner, G. Kazakov, and H. Ritsch, "Code 3: 6-level atom repumping example program," figshare (2022), https://doi.org/10.6084/m9.figshare.18095861.